THE ASTROPHYSICAL JOURNAL, 516:704–715, 1999 May 10

PROBING THE DUST-ENSHROUDED REGIONS OF THE INTERACTING GALAXY SYSTEM ARP 299: A NEAR-INFRARED STUDY

S. SATYAPAL,[1] D. M. WATSON, W. J. FORREST, AND J. L. PIPHER
Department of Physics and Astronomy, University of Rochester, Rochester, NY 14627; satyapal@stars.gsfc.nasa.gov
J. FISCHER
Remote Sensing Division, Naval Research Laboratory, Code 7600, 4555 Overlook Avenue, Washington, DC 20375
M. A. GREENHOUSE
Goddard Space Flight Center, Code 685, Greenbelt, MD 20771
H. A. SMITH
Harvard-Smithsonian Center for Astrophysics, 60 Garden Street, Cambridge, MA 02138
AND
CHARLES E. WOODWARD[2]
Department of Physics and Astronomy, University of Wyoming, Laramie, WY 82701-3905
Received 1998 June 16; accepted 1998 December 10

ABSTRACT

We present high spectral resolution ($\lambda/\delta\lambda \cong 10^3$) Pa$\beta$(1.28 μm) and Brγ(2.17 μm), 3.29 μm dust feature, and near-infrared broadband images of the Arp 299 = NGC 3690/IC 694 galaxy system. The emission is found to be concentrated at the positions of three active regions, known as sources A, B, and C. From our Brγ/Paβ flux ratio we find the visual extinction toward the ionized gas in A, B, and C is $\sim$6, 6, and 2 magnitudes, respectively, assuming case B recombination and a foreground screen geometry for the obscuring material. Our observations can be explained entirely by a starburst model for the Arp 299 system. The putative active galactic nucleus (AGN) in source A does not dominate the properties of this source. We see no evidence of broad recombination lines. In addition, the ratio of the 3.29 μm dust feature to total luminosity, a tracer of starburst activity, is consistent in each source with that seen in M82 and other starburst galaxies. Also, our imaging observations reveal that the dust feature emission is concentrated in the nucleus of source A, contrary to the extended annular distribution of the feature emission seen surrounding the nucleus of the more distant Seyfert galaxy NGC 7469. In this galaxy, the absence of the feature emission in the nucleus has been attributed to the destruction of the dust carriers in the hard radiation field surrounding the AGN. Our observations suggest that all of the active regions in Arp 299 are characterized by starburst episodes. The observed CO indices and Brγ equivalent widths imply that source B is older than source A and source C is the youngest star-forming region. Although these regions are probably complex physical systems not necessarily characterized by a single coeval population of stars, we have compared our observations with an instantaneous starburst model with a Salpeter initial mass function. Using this simple model, we find starburst ages of $\sim 6 \times 10^6$, 8×10^6, and 4×10^6 for sources A, B, and C, respectively.

Subject headings: galaxies: individual (Arp 299) — galaxies: nuclei — infrared: galaxies — infrared: ISM: lines and bands

1. INTRODUCTION

Infrared luminous galaxies are an important class of extragalactic objects. In addition to being the dominant population of extragalactic objects in the local universe at the most extreme luminosities ($L > 10^{12}\ L_\odot$; Sanders & Mirabel 1996), infrared luminous galaxies appear to be linked to a number of scientific research areas of fundamental importance, including globular cluster formation, the formation of elliptical galaxies, and the formation of quasars. Also, since infrared bright galaxies are thought to be local analogs of protogalaxies (Stark 1997), a detailed understanding of these objects will provide important information for future high-z studies and galaxy formation models.

An order of magnitude more luminous than the prototypical starburst galaxy M82 and half as luminous as the galaxy Arp 220, Arp 299 bridges the gap between nearby well-studied starburst galaxies and the more enigmatic ultraluminous galaxies. Study of this system therefore provides us with the unique opportunity to investigate the differences and possible connections between local starbursts and higher luminosity systems. With a far-infrared luminosity of $5.2 \times 10^{11}\ L_\odot$ (Soifer et al. 1987), Arp 299 consists of the two galaxies NGC 3690 and IC 694. An interaction between two gas-rich spiral galaxies is suggested by the visible knots and filaments observed in the system (de Vaucouleurs & de Vaucouleurs 1967). However, the lack of large-scale tails, which are often associated with evolved interacting galaxy systems (see, e.g., Toomre & Toomre 1972), suggests that Arp 299 is a young interacting system (Bushouse & Gallagher 1984). The measured radial velocity of 3159 km s^{-1} (Sanders & Mirabel 1985) corresponds to a

[1] Current address: Goddard Space Flight Center, Code 685, Greenbelt, MD 20771.
[2] NSF Presendential Faculty Fellow.

distance of 42 Mpc for a Hubble constant of 75 km s^{-1} Mpc^{-1}. CO observations show that the system contains a large mass of molecular hydrogen ($\sim 3 \times 10^9$ $M_\odot$, assuming a Galactic molecular gas conversion factor; Sargent et al. 1987). Gehrz, Sramek, & Weedman (1983, hereafter GSW) found strong 10 μm, radio, and Hα emission from Arp 299, which suggests the presence of several sites of vigorous star formation activity.

In this article, we carry out a detailed near-infrared study of Arp 299. High spatial resolution spectroscopic and broadband observations are used to constrain and compare the starburst properties in each of the active regions in this system.

2. OBSERVATIONS AND DATA REDUCTION

2.1. *Near-Infrared Broadband Images*

Broadband observations of Arp 299 were made with the University of Rochester's 58×62 InSb infrared array camera at the Mount Lemmon Observing Facility (MLOF) 60 inch (1.5 m) telescope. Observations at J(1.23 μm), H(1.65 μm), and K(2.23 μm) were carried out in 1992 January. All images were linearized, background-subtracted, divided by morning sky flats at the same wavelength, spatially registered and aligned using a cross correlation procedure, and co-added. Flux calibration was achieved using the standard star HD 7721 (Elias et al. 1982). The estimated uncertainty in these broadband measurements is 15%. The final images at each wavelength have a plate scale of 0.089 $pixel^{-1}$.

2.2. *3.3 Micron Narrowband Images of Arp 299*

Narrowband 3.3 μm imaging of Arp 299 was carried out in 1995 June at the Wyoming Infrared Observatory (WIRO) 2.34 m telescope with the University of Rochester Third Generation Array Camera and a 1.85% bandwidth CVF (equivalent width resulting from the convolution of the Gaussian CVF profile with 0.8% resolution and a circular Lyot-stop profile). Images with 1 s integration times and 128 co-adds were taken at 3.158 and 3.326 μm (redshifted line-center). The data set consisted of 16 on-line images and 16 continuum frames. On-chip nodding was carried out in all observations to double our efficiency. The spatial resolution of our data was 1.″2. All images were linearized, background-subtracted, and divided by sky flat fields at the same wavelength. The standard star σ Cyg ($m_K = 3.795$) was used for calibration. Spatial registration and co-addition was carried out using the same methods that were applied to the broadband data. Since the instrumental width is comparable to the width of the 3.29 μm dust, feature, the feature flux was calculated by assuming that the 3.29 μm feature profile in Arp 299 is the same as that obtained for the inner 2.″6 of M82 from Tokunaga et al. (1991). Assuming an equivalent width for the feature of 0.05 μm, and using our instrumental equivalent width of 0.065 μm, the 3.158 μm continuum image was subtracted from the line center image and the result was multiplied by the equivalent width corresponding to the convolution of the instrumental and dust feature widths (0.082 μm).

2.3. *Arp 299 Recombination-Line Images*

Hydrogen recombination-line observations of Arp 299 were made at WIRO with the University of Rochester Third Generation Array Camera and the NASM/NRL Fabry-Perot interferometer (FPI) systems (see Satyapal et al. 1995; Greenhouse et al. 1997). Images at a total of seven different FPI cavity positions (z), at 100 s integration time per image, centered on the redshifted Paβ line ($v = 3159$ km s^{-1}) were obtained on 1994 May 11. The on-line point spacing was 1/3 $(\delta\lambda)_{\rm FWHM}$, and the off-line continuum images were at $\pm 5(\delta\lambda)_{\rm FWHM}$ from line center. Four such data sets were recorded. The Brγ observations were obtained on 1994 May 16. This data set consisted of images at nine different z positions, again with on-line point spacing of 1/3 $(\delta\lambda)_{\rm FWHM}$ and off-line point spacing of $\pm 5(\delta z\lambda)_{\rm FWHM}$. Two such data sets were obtained. Early morning sky frames at each of the wavelengths were again used as flat fields. The images were calibrated using the standard star BS 4550 (G8 V; $m_K = 4.385$). Alignment and spatial registration of the images was again accomplished using the same cross-correlation procedure. Wavelength calibration was obtained by observing argon and krypton lamp lines closely bracketing the hydrogen recombination lines. Finally, nonlinear fitting to an Airy function and correction for the dispersion in the peak wavelength of transmission across the array (see Cole 1996; Greenhouse et al. 1997) allowed us to extract images of the total line flux, observed line wavelengths, line widths, and the continuum flux density.

3. RESULTS

Our K-band image is shown in Figure 1. The near-infrared emission, in addition to the mid-infrared (Keto et al. 1997) and radio emission (Zhao et al. 1997), originates primarily in three regions, labeled by GSW as sources A, B, and C. Source A corresponds to the nucleus of IC 694 (Telesco, Decher, & Gatley 1985). Source B is a double source with source B1 being the nucleus of NGC 3690 (Wynn-Williams et al. 1991). The nuclear separation is $\sim 21''$, or 4.3 kpc in projection. Source C is not clearly identifiable with either galaxy's nucleus and is thought to be a product of the interaction. Our Paβ(1.28 μm) and Brγ(2.17 μm) images appear in Figure 2. Figure 3 is our 3.29 μm dust feature image of Arp 299, along with the corresponding 3 μm continuum image.

Our recombination-line fluxes along with a selection of previously published emission-line fluxes are listed in Table 1. Table 2 is a summary of our 3.29 μm photometry in comparison with previous results.

Our recombination-line spectrophotometry is in reasonably close agreement with previous measurements. Pointing differences between single-aperture observations and our synthetic apertures can result in the minor discrepancies observed. The Brγ line profiles corresponding to the flux in a 5″ aperture centered on each of the sources are shown in Figure 4.

3.1. *Extinction toward Arp 299*

The extinction toward the ionized gas in Arp 299 can be estimated from the observed ratios of recombination lines. Assuming case B recombination applies and $T_e = 10^4$ K and $n_e = 10^2$ cm^{-3}, the intrinsic Paβ/Brγ line flux ratio is 5.84 (Hummer & Storey 1987). We assume a $\tau_\lambda \propto \lambda^{-1.85}$ (Landini et al. 1984) extinction law and that the obscuring material can be treated as a foreground screen. At a distance of 42 Mpc, our spatial resolution corresponds to approximately 200 pc. A uniform foreground screen assumption is therefore probably an oversimplification. However, we can obtain estimates of the extinction to the

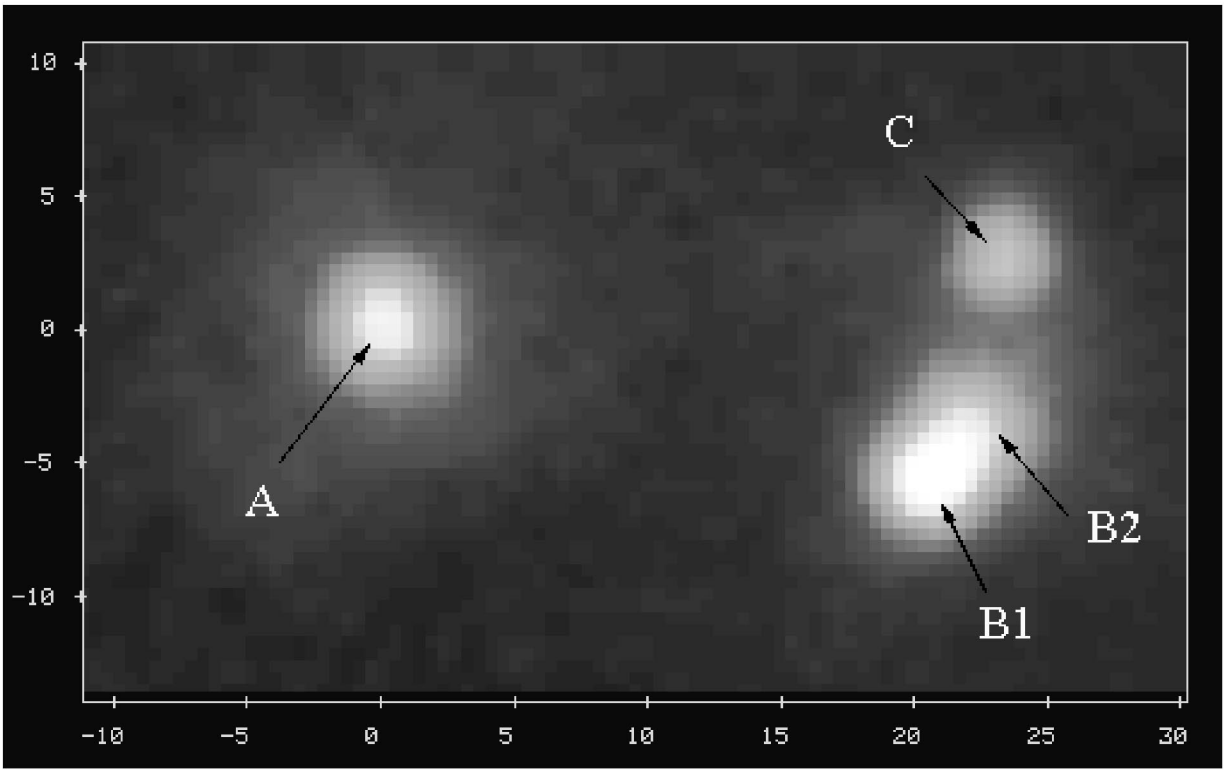

FIG. 1.—*K*-band image of Arp 299. Tick marks correspond to 5″ intervals relative to source A.

bulk of the ionized gas, which allows us to obtain global information about the star formation activity in each of the active regions in Arp 299. Our derived extinctions are listed in Table 3 along with previously published results. The extinction toward sources A, B, and C was calculated using the total Paβ and Brγ fluxes in a 5″ synthetic aperture centered on each of the sources. In order to assess the dependence of the derived extinction on beam size for the range of apertures used in the literature, our recombination line fluxes in synthetic apertures ranging from 1″ (200 pc) to 10″ (2 pc) centered on each of the sources were used to derive the extinction. For these apertures the derived extinction toward each of the sources was found to vary by less than 17%, which would correspond to a difference of at most a factor of 1.1 in the dereddened Brγ flux. In order to test the validity of an $\alpha = 1.85$ extinction power law, we used our Brγ and Paβ fluxes in sources A and B to predict the Brα flux and compared this value to that measured by Beck, Turner, & Ho (1986). In a 7.″2 aperture, our Brγ flux is 7.8×10^{-17} W m^{-2} and our Paβ flux is 1.32×10^{-16} W m^{-2} at the position of source A. If we assume an $\alpha = 1.85$ extinction power law, the optical depth at $\lambda_{\mathrm{Br}\gamma}$ is 0.78 and 0.25 at $\lambda_{\mathrm{Br}\alpha}$. The predicted intrinsic Brα line flux is then 4.8×10^{-16} W m^{-2}, corresponding to an observed flux of 3.7×10^{-16} W m^{-2}. This value is within 1 σ of the flux measured by Beck et al.. At the position of source B, the predicted intrinsic Brα line strength is 3.9×10^{-17} W m^{-2}, which corresponds to an observed flux of 3.2×10^{-16} W m^{-2}, also within 1 σ of the measured value. Power-law indices less than 2 result in predicted Brα line strengths that are within 1 σ of the observed flux. Thus, the near-infrared recombination-line measurements do not constrain tightly the extinction law in Arp 299. An extinction law flatter than the $\alpha = 1.85$ power law can be produced by a variation in the extinction on scales smaller than a 7.″2 aperture and does not necessarily imply an anomaly in the grain properties of the obscuring material.

Substantial variation is seen in the derived extinctions toward sources A, B, and C reported in the literature. Table 3 summarizes a selection of these results. Zhao et al. (1997) have observed the H92α radio recombination line in sources A and B. At these wavelengths, non-LTE effects become important. Using the observed recombination line flux from sources A and B, Zhao et al. model the physical conditions of the ionized gas. Using the measurement of only one radio recombination line, the derived ionizing photon rate and excitation parameter for the gas are not determined uniquely. These quantities are dependent on several parameters such as the electron density, electron temperature, the geometry, size, and total number of H II regions. Assuming an electron temperature of 5000 K and a distance to Arp 299 of 40.3 Mpc, they derive a range for the ionizing photon rate of 3.8–4.6 $\times 10^{54}$ s^{-1} for source A. Using our observed Brγ flux, adopting the same distance and electron temperature, we find an ionizing photon rate of 7.3×10^{53} s^{-1}, which would imply a higher extinction ($A_v \sim 15$–17 mag) than that derived using our near-infrared recombination line observations. For source B, the radio recombination line flux results in an ionizing photon rate of 1.5–8.8 $\times 10^{53}$ s^{-1}, compared with 4.4×10^{53} s^{-1} obtained using our observed Brγ flux. This implies an extinction toward source B of $A_v > 7$ mag, consistent with our result.

The extinction derived using the CO ($J = 1 \rightarrow 0$) column density gives a much larger value for the extinction toward sources A and C compared with source B. Sargent et al. (1987) find $N(\mathrm{H_2})_{\mathrm{A}} = 1.1 \times 10^{23}$ cm^{-2}, $N(\mathrm{H_2})_{\mathrm{B}} = 2.4 \times 10^{22}$ cm^{-2}, and $N(\mathrm{H_2})_{\mathrm{C}} = 1.1 \times 10^{23}$ cm^{-2}, assuming a CO to $\mathrm{H_2}$ conversion factor of 3.6×10^{20} $\mathrm{H_2}$ cm^{-2} (K km

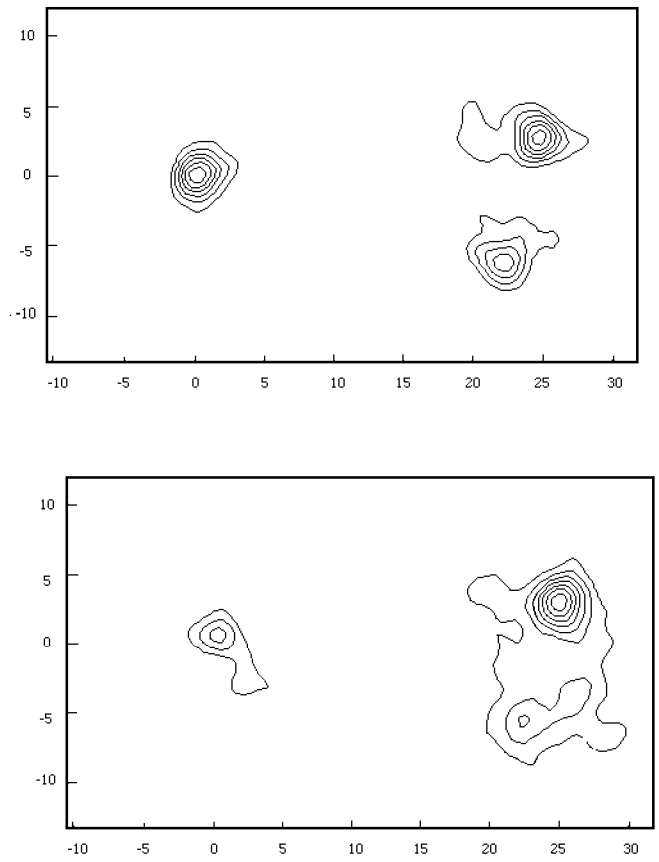

FIG. 2.—Hydrogen recombination-line images of Arp 299. *Top*: Brγ image contoured from 2×10^{-18} to 4×10^{-18} W M^{-2} arcsec^{-2} in intervals of 5×10^{-19} W m^{-2} arcsec^{-2}. *Bottom*: Paβ image contoured from 5×10^{-18} to 2×10^{-17} W m^{-2} arcsec^{-2} in intervals of 2×10^{-18} W m^{-2} arcsec^{-2}.

s^{-1})$^{-1}$. For N(H I) = $2N(H_2)$ and $N(H)/A_K = 1.89 \times 10^{22}$ cm^{-2} (Draine 1989), $A_{V_A} = 58$, $A_{V_B} = 13$, $A_{V_C} = 58$. Uncertainties in the CO/H_2 column density ratio, the CO line optical depth, the gas to dust ratio, and the fraction of CO column density that is in front of the ionized gas in sources A, B, and C, makes comparisons between these values and those obtained using the recombination-line measurements questionable. Shier, Rieke, & Rieke (1994) have used observations of the 2.3 μm absorption bands of CO to derive a dynamical mass within the central region of IC 694 (source A). This mass is 4–10 times less than the H_2 mass determined from the observed CO ($J = 1$–0) fluxes and the standard molecular gas conversion factor, which would reduce the estimates of the extinction derived from the CO column density. If the molecular gas conversion factor is the same in all three sources, and the gas to dust ratio is also the same, a large fraction of molecular material is behind the ionized gas in sources A and C, in contrast to B, for a simple screen model.

Nakagawa et al. (1989) measured the H_2 $v = 1$–0 $S(1)$ and $v = 1$–0 $Q(3)$ lines in a 5″ aperture centered on source A. Since these lines arise from the same upper state, their ratio is independent of temperature and density and can thus be used to determine the extinction. The intrinsic ratio is 0.7 and the observed ratio is 0.5 in source A, indicating $A_v <$ 8.5 mag, consistent with our result.

3.2. *The 3.29 Micron Dust Feature Emission in Arp 299*

As can be seen in Figure 3, the 3.29 μm dust feature emission is detected in sources A, B1, and C. The 3.29 μm feature emission has been found to be well correlated with the FIR luminosity in a number of starburst galaxies (e.g., Dennefeld & Desert 1990; Mouri et al. 1990). We have calculated the 3.29 μm feature to total FIR luminosity ratio in each of the sources in Arp 299 and compared them with the value in M82 (Satyapal et al. 1995); the results appear in Table 4. The far-infrared luminosities of the sources were estimated using the far-infrared luminosity of 5.2×10^{11} $L_\odot$ measured by *IRAS* (Soifer et al. 1987) and the higher spatial resolution 50 and 100 μm observations by Joy et al. (1989), which showed that 60% of the total FIR luminosity from Arp 299 comes from source A.

The extinction-corrected dust feature flux values were calculated as follows. The uncorrected flux in a 5″ aperture centered on source A was subtracted from the total uncorrected flux in a 20″ aperture centered on this source. The resulting flux was then added to the extinction-corrected 5″ flux, using the extinction derived from the recombination-line data. This was taken to represent the total, extinction-corrected flux from source A. It should be noted that this is probably a lower limit to the total feature flux since we have not applied an extinction correction to the low-level, diffuse 3.29 μm feature emission outside the region probed by the recombination-line data. A similar procedure was applied to the fluxes from sources B and C; in this case, the 3.29 μm flux from each source was dereddened separately, using the extinction corresponding to each source. As can be seen in Table 4, the extinction-corrected FIR to 3.29 μm luminosity ratio is somewhat higher in Arp 299 than in M82, although it should be pointed out that this ratio is less accurate in Arp 299, where the assumptions used to correct for extinction are less reliable. It is interesting to note that the 3.29 μm dust feature emission appears to be a better indicator of the FIR luminosity in the Arp 299 system than is the hydrogen recombination-line emission. The extinction-corrected FIR to Brγ luminosity ratio is 7.0×10^4 in source A and 2.6×10^4 in sources B and C combined. Since the dust feature carriers can be excited by ionizing and lower energy photons while the Brγ emission requires ionizing photons, this feature is not as sensitive to the radiation field of the starburst and is thus a better indicator of the FIR luminosity.

As can be seen from Table 4, the 3.29 μm feature to total FIR luminosity ratio in Arp 299 is comparable to that seen in the prototypical starburst, M82, which suggests that an AGN does not dominate the properties of any of the active regions. Furthermore, the centrally condensed 3.29 μm feature emission observed from each source is also contrary to the existence of a prominent AGN in Arp 299. The Seyfert galaxy NGC 7469, known to possess circumnuclear star formation activity and an AGN, shows an extended annular region of 3.29 μm (Mazzarella et al. 1994; Nelson et al. 1999) and 11.3 μm (Miles, Houck, & Hayward 1994) dust feature emission around the nucleus. In this galaxy, the absence of the feature emission in the nucleus has been attributed to the destruction of the dust carriers in the hard radiation field surrounding the AGN. The annulus of 3.29 μm dust feature emission in NGC 7469 has an inner radius of 2″ east-west by ~1″ north-south, and an outer radius of 3.″7 north-south by 4.″6 east-west (Nelson et al.). If Arp 299

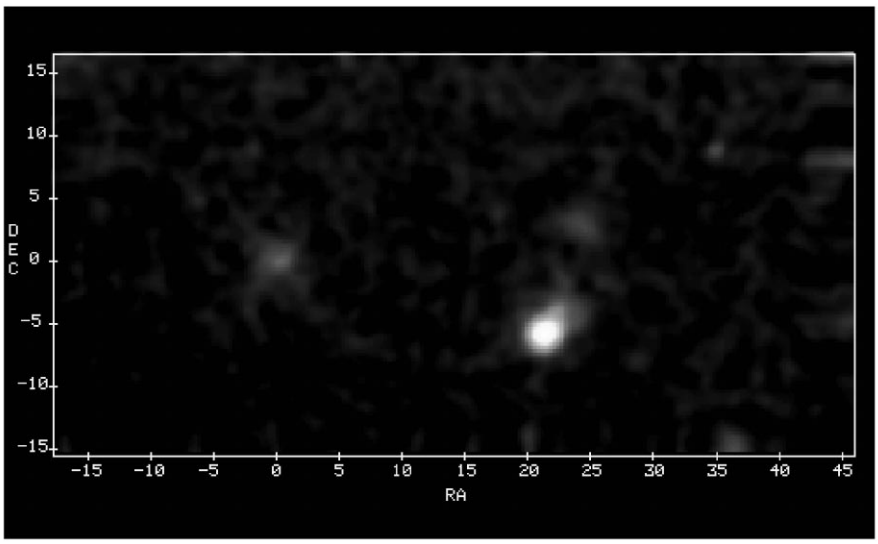

FIG. 3*a*

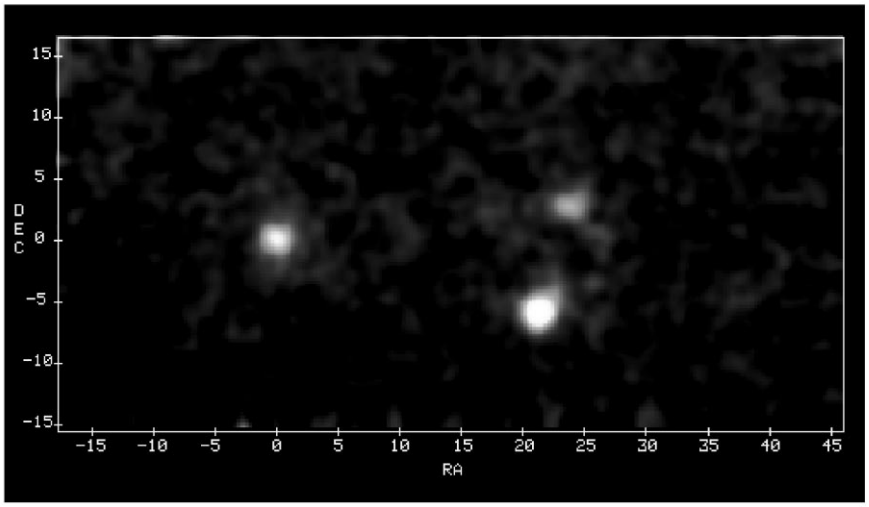

FIG. 3*b*

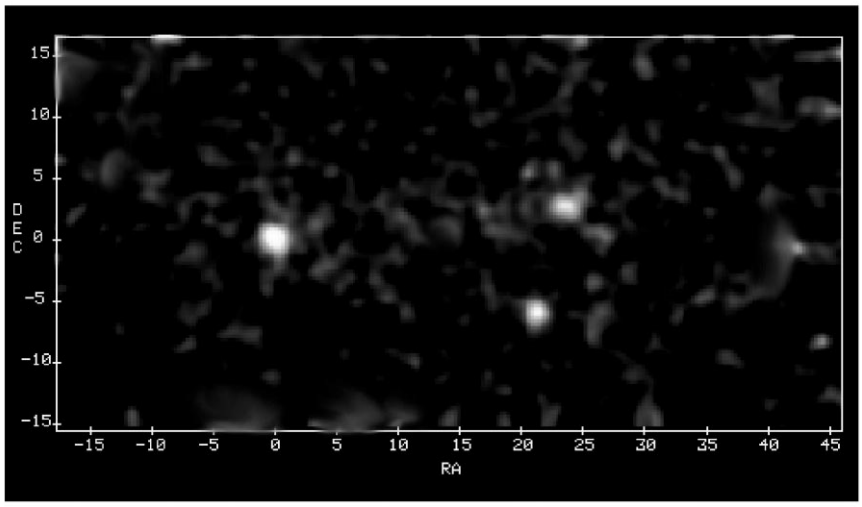

FIG. 3*c*

FIG. 3.—Gray-scale images of the emission near 3.3 μm from Arp 299. (*a*) 3.159 μm continuum image displayed from 2×10^{-18} to 1.2×10^{-16} W m^{-2} μm^{-1} pixel^{-1}. (*b*) 3.326 μm continuum + feature image displayed from 2×10^{-18} to 1.8×10^{-16} W m^{-2} μm^{-1} pixel^{-1}. (*c*) Continuum-subtracted image displayed from 1×10^{-19} to 6.2×10^{-18} W m^{-2} pixel^{-1}.

TABLE 1

SELECTION OF EMISSION-LINE MEASUREMENTS IN ARP 299

Line	λ (μm)	Aperture Diameter (arcsec)	Position	Observed Flux[a] (10^{-17} W m^{-2})	Reference
Hβ	0.486	3.6	A	<7	1
			B	7.9	1
			C	22	1
Hα.....	0.656	3.6	A	<20	1
			B	50	1
			C	120	1
Paβ.....	1.282	7.2	A	13.2	2
			B	17.4	2
		5	A	11.7	2
		5	B	8.6	2
		5	C	21.4	2
Brγ	2.167	7.2	A	6.1 ± 1.6	3
			B	<4.6	3
			A	7.8	2
			B	7.6	2
		5.5×5.5	A	4.1 ± 0.7	4
		5.5×7.0	B	3.2 ± 0.4	4
		4.7×4.7	C	4.1 ± 0.4	4
		5	A	5.02	2
		5	B	4.03	2
		5	C	4.77	2
		2.7	A	1.9 ± 0.7	5
			B	<1.7	5
			C	4.1 ± 1.2	5
		2.7	A	3.42	2
			B	2.01	2
			C	2.97	2
Brα	4.051	7.2	A	48 ± 11	3
			B	40 ± 11	3

[a] We estimate a 20% uncertainty in our spectrophotometry.

REFERENCES.—(1) GSW; (2) this work; (3) Beck et al. 1986; (4) Fischer et al. 1990; (5) Nakagawa et al. 1989.

contains an AGN comparable to the one in the more distant galaxy NGC 7469 ($d \sim 65$ Mpc), a similar annulus would have been revealed by our $\sim 1''$ spatial resolution observations.

3.3. *Near-Infrared Broadband Emission*

The observed near-infrared colors of the three sources are quite different from one another, as can be seen in Figure 5. We have plotted the observed colors obtained from the total near-infrared fluxes in $5''$ apertures centered on each source. Also plotted are the colors of normal stars (Koornneef 1983) and the reddening vector indicating the effect of foreground extinction. Applying the extinction derived from the recombination-line measurements to the near-infrared emission is probably an oversimplification; the extinction toward the ionized gas is not necessarily applicable to the near-infrared broadband emission in Arp 299. Also, the foreground screen assumption is also not necessarily realistic in this case. All three sources have colors that deviate substantially from the colors of normal stars. We have also calculated the contribution to the near-infrared continuum from free-free and free-bound processes

TABLE 2

PHOTOMETRY FOR THE 3.291 MICRON FEATURE IN ARP 299

Author	Aperture[a] (arcsec)	Position	$S_{3.159}$ [W m^{-2} μm^{-1} ($\times 10^{-15}$)][b]	$F_{3.326}$ [W m^{-2} ($\times 10^{-16}$)]
Dennefeld & Desert 1990	2.7	A	5	5.0 ± 0.9
Mizutani, Suto, & Maihara 1994.....	5.4×7.3	A	8	5.8 ± 1.6
		B	20	7.4 ± 1.5
		C	7	4.3 ± 1.5
This work[c]	2.7	A	2.50	3.23
	7.1	A	7.05	8.53
	7.1	B	18.7	2.69
	7.1	C	4.37	6.33

[a] Our photometry was done with circular apertures with specified diameter.

[b] The continuum level was estimated from the information provided in the indicated reference.

[c] We estimate a 15% error in our photometry.

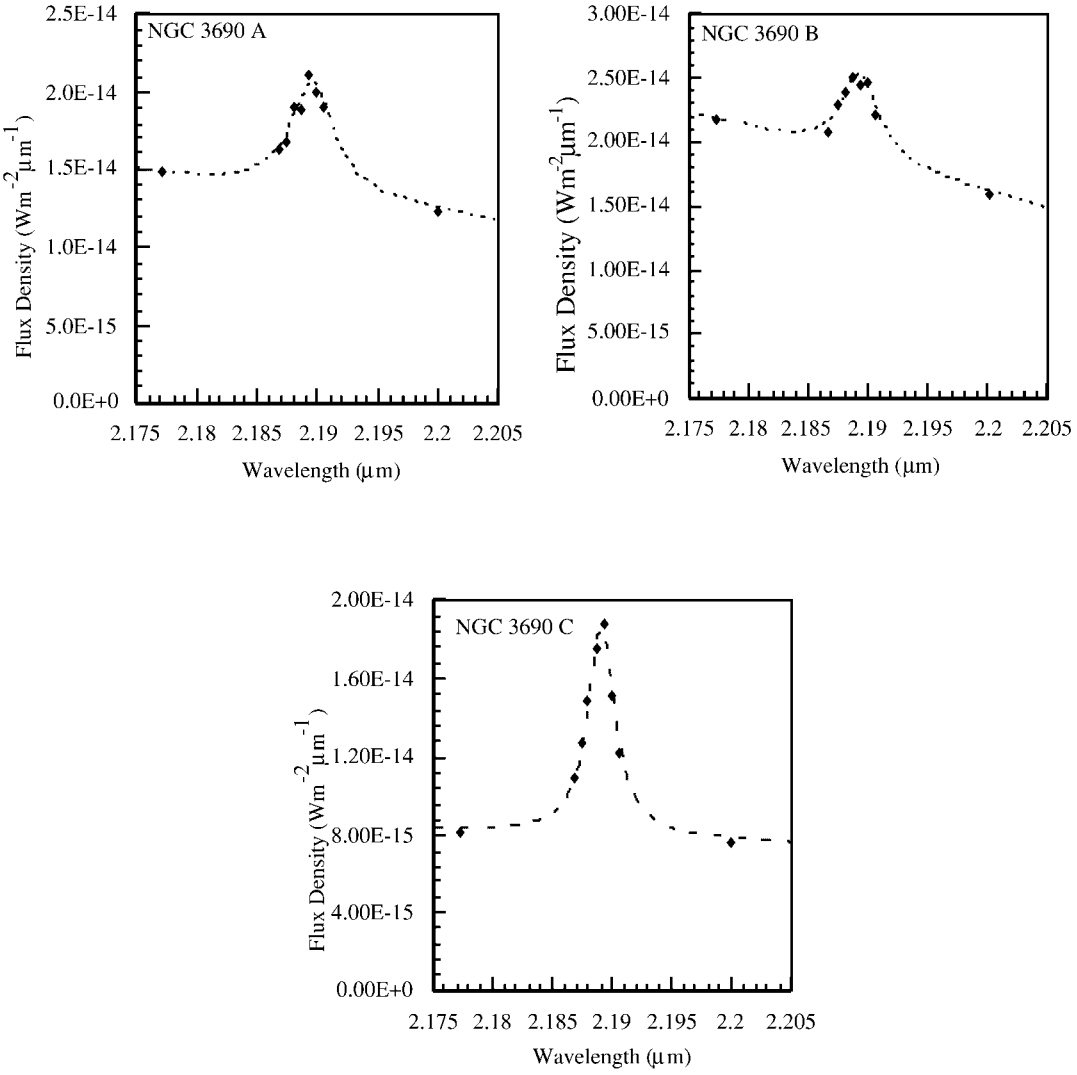

FIG. 4.—Brγ line profile from a 5″ aperture centered on each of the active regions in Arp 299. Dashed line corresponds to the Lorentzian fit to the data. The lines are not resolved in any of the sources. The instrumental line width is $(\delta\lambda)_{\rm FWHM} = 0.0025$ μm.

(see Satyapal 1995). In source A, these processes are found to contribute 3%, 4%, and 6% to the extinction-corrected J(1.25 μm), H(1.65 μm), and K(2.2 μm) emission, respectively. In source B, the contributions are 2%, 3%, and 4%, and in source C, the contributions are 17%, 12%, and 10%. These processes are found to be the most significant in source C.

We can also estimate the contribution to the near-infrared continuum from transiently heated small particles ("hot" dust). The near-infrared emission from a collection

TABLE 3

EXTINCTION (A_V) TOWARD ARP 299

Method	Beam (arcsec)	Source A (mag)	Source B (mag)	Source C (mag)
Hβ/Hα[a]	3.6	...	2.4	1.9
Paβ/Brγ[b]	5	5.6	6.2	1.6
Brγ/Brα[c]	7.2	13	14	...
H_2 $S(1)/Q(3)$[d]	5	<8.5	...	...
Silicate[a]	5	24	14	5.5
N_{H_2}[e](from CO).....	5	58	13	58
H92α/Brγ[f]	3.5	~15–17	<7	...

[a] Gehrz, Sramek, & Weedman 1983.
[b] This work.
[c] Beck et al. 1986.
[d] Nakagawa et al. 1989.
[e] Sargent et al. 1987.
[f] Zhao et al. 1997.

TABLE 4

THE 3.29 MICRON DUST FEATURE EMISSION AND THE FIR EMISSION IN ARP 299: COMPARISON WITH M82

Source Luminosity	Position A	Position B + C	M82 (30″ aperture centered on nucleus)
$L_{FIR}(10^{11}\ L_\odot)$.....	3.3	1.9	0.44
$L_{3.3}(10^8\ L_\odot)$.....	1.01	1.15	0.26
$L_{3.3}^{corr}(10^8\ L_\odot)$	1.80	1.23	0.33
$L_{FIR}/L_{3.3}$	3280	1650	1690
$(L_{FIR}/L_{3.3})^{corr}$	1840	1550	1340
$(L_{FIR}/L_{Br\gamma})^{corr}$	7.0×10^4	2.6×10^4	1.38×10^4

of small particles transiently heated by the absorption of ultraviolet and visible photons resembles that of a graybody with color temperature 1000 K (see, e.g., Sellgren, Werner, & Dinerstein 1983). Sellgren et al. have shown that the 3.29 μm line to continuum ratio is roughly constant (~ 6) at several locations in a number of reflection nebulae. Using the extinction-corrected 3.29 μm feature fluxes in a 5″ aperture centered on sources A, B, and C ($F_{A3.3}^{corr} = 8.38 \times 10^{-16}$ W m^{-2}; $F_{B3.3}^{corr} = 4.85 \times 10^{-16}$ W m^{-2}; $F_{C3.3}^{corr} = 5.68 \times 10^{-16}$ W m^{-2}), and assuming a feature to continuum ratio of ~ 6, the extinction-corrected emission due to hot dust at 3.3 μm can be obtained ($F_{A3.3dust}^{corr} = 1.64 \times 10^{-15}$ W m^{-2}; $F_{B3.3dust}^{corr} = 9.62 \times 10^{-16}$ W m^{-2}; $F_{C3.3dust}^{corr} = 1.13 \times 10^{-15}$ W m^{-2}). Assuming that the hot dust continuum can be approximated by a 1000 K graybody, the extinction-corrected J, H, and K flux densities can be obtained. Hot dust emission is found to contribute 0%, 2%, and 7% to the extinction-corrected J, H, and K emission, respectively, in source A. In source B, the contributions are 0%, 1%, and 3%, and in source C, the contributions are 1%, 6%, and 12%. It should be pointed out that the feature to continuum ratio used may not be applicable in Arp 299; therefore, these estimates for the hot dust emission should be viewed with some caution.

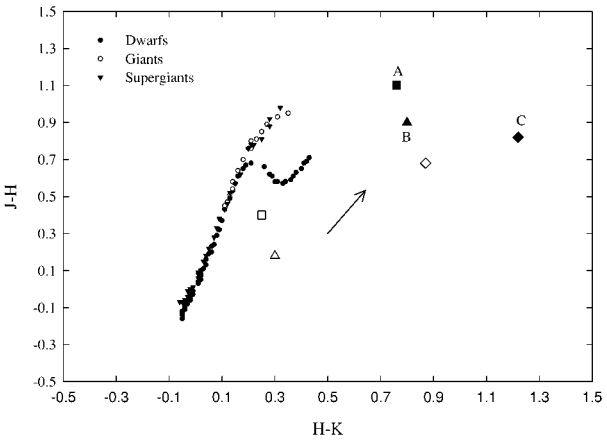

FIG. 5.—Two-color diagram for the Arp 299 system. The colors of dwarf, giant, and supergiant stars are plotted with the symbols indicated on the figure. Filled symbols represent the colors of sources A, B, and C, and the corresponding open symbols represent the positions after an extinction correction has been applied and the nebular continuum subtracted. The nebular continuum is the estimated free-free, free-bound, and "hot" dust emission from each source. The length of the reddening vector corresponds to $A_V = 2$.

The positions of the compact sources in Arp 299 on a two-color diagram (Fig. 5) are significantly different from those of normal stars. Sources A and B have foreground-extinction-corrected colors similar to those of the pointlike sources in M82 (Satyapal et al. 1997). These colors can easily be moved to the positions of normal stars with a slight change in the assumed dust geometry (see Satyapal et al. 1997). Source C, however, has a very unusual color that cannot be ascribed to extinction from any assumed dust geometry. There is a possible detection of Wolf-Rayet features in a broad emission band near 4660 Å from this source but not from sources A and B (Armus, Heckman, & Miley 1989). Wolf-Rayet stars in our Galaxy are observed to have colors very similar to those of source C (Williams, Van der Hucht, & The 1987), which suggests that the colors of source C can be understood as the combined effects of a population of Wolf-Rayet stars, normal stars, and dust emission. We have not estimated the contribution to the near-infrared continuum from warm dust emission. If the 12 μm emission provides some indication of the warm dust component, comparing the 12 μm to K flux ratio may provide some indication of the relative importance of warm dust emission to the near-infrared colors in sources A, B, and C. This ratio is ~ 25, 30, and 18 in sources A, B, and C, respectively (inferred using the 4″ 12.5 μm observations from Keto et al. 1997). Assuming that the 12 μm emission does correlate with the warm dust emission, it would appear that the unusual colors of source C cannot be explained by the thermal emission from warm dust alone.

3.4. *Comparisons between Each of the Compact Sources*

Each of the compact sources in Arp 299 exhibits significantly different observed properties, as can be seen in Table 5. The spatial distribution and temperature of the dust appear to be peculiar in Arp 299. As previously mentioned, source A has the largest FIR luminosity even though the Brackett line fluxes (and extinction) are comparable in sources A and B. Source A also has the highest 3.29 μm dust feature flux. The 10 μm flux density from B, on the other hand, is a factor of 2 larger than that from A (GSW). Finally, the relative positions of each of the sources on a two-color diagram (Fig. 5) is suggestive of an increase in the contribution of near-infrared dust emission in source B compared with A and in source C compared with B.

Ridgway, Wynn-Williams, & Becklin (1994) have measured the CO $\Delta v = 2$ bandhead strength in sources A, B, and C. Each of the sources is found to have substantially different absorption depths. The 2.3 μm CO absorption feature, observed from the atmospheres of late-type stars, is

TABLE 5

SUMMARY OF MAIN PROPERTIES OF ARP 299

Property	Source A	Source B	Source C
L_{FIR}[a](10^{11} $L_\odot$)	3.3	1.9	1.9
M_{H2}[b](10^8 $M_\odot$)	14	<3	14
N_{UV}[c](10^{54} s^{-1})	1.4	1.2	0.94
$S_{12.5\mu m}$[d](mJy)	410	540	170
$H-K$(observed)[e]	0.76	0.80	1.22
CO index[f]	0.17	0.07(B1), 0.21(B2)	0.06
$S_{5\ GHz}$[g](mJy)	160	30	
Thermal $S_{5\ GHz}$[h](mJy)	10	8	7
α[g]	−0.34	−0.80	−0.89
H_2 1–0 $S(1)$/Brγ[i]	1.66	1.84	0.49
He I 2.06 μm/Brγ[j]	0.557	0.381	0.536

[a] Soifer et al. 1987, and Joy et al. 1989.
[b] Sargent et al. 1987.
[c] Derived from this work.
[d] Flux in 4″ aperture centered on each source from Keto et al. (1997).
[e] This work.
[f] Ridgway et al. 1994. Converted from spectroscopic to photometric CO index.
[g] Inferred from contour map in GSW. Spectral index from 6 and 20 cm observations from GSW.
[h] Inferred from this work.
[i] Fischer et al. 1990.
[j] Doherty et al. 1995.

dependent on the stellar luminosity and temperature (Frogel et al. 1978; Kleinmann & Hall 1986). The CO index of normal galaxies is 0.15 (Frogel et al. 1978). As can be seen from Table 5, source A has a slightly higher than normal CO index while source C shows no CO absorption. Source B2 has a high CO index while source B1 shows no CO absorption. Shallower depths can artificially be produced by the contamination of the K-band continuum by non-stellar processes (e.g., free-free and free-bound processes and the emission from hot dust). Our estimates of the nebular continuum discussed above can be used to calculate the intrinsic CO absorption depths given the observed indices. The derived intrinsic CO index is 0.20 in source A and 0.22 in source B2. Thus, the differences in the observed CO index in sources A, B, and C appears to be attributable to differences in the IMF or age of the starburst stellar populations.

Information about the IMF or age of a star formation region is given by the ionizing photon rate per unit total luminosity. More massive O stars give a smaller ratio of L_{FIR}/N_{UV}. Hence a young coeval stellar population (younger than $\sim 10^6$ yr, the lifetime of O5 main-sequence stars) characterized by an IMF continuing to very high masses will show a lower ratio than a young population characterized by an IMF with a lower upper mass cutoff. On the other hand, for a given IMF, a larger ratio of the FIR luminosity to ionizing photon rate can be produced by a difference in the age of the starburst: the stellar population in an older burst would be comprised of fewer very massive stars, thereby producing fewer ionizing photons. From Table 5, L_{FIR}/N_{UV} is much larger in source A compared with B and C. Thus B+C are either younger or the IMF of the stellar population has a higher upper mass cutoff than in source A. These interpretations have been suggested previously (e.g. Telesco et al. 1985; Nakagawa et al. 1989). The ionizing photon rate was derived using the extinction-corrected Brγ flux in a 5″ aperture centered on each source, with the assumed foreground obscuring screen and an $\alpha = 1.85$ extinction power law ($F_{Br\gamma A} = 5.02 \times 10^{-17}$ W m^{-2}; $F^{corr}_{Br\gamma A} = 8.88 \times 10^{-16}$ W m^{-2}), and the assumption of case B recombination. The resulting Lyman continuum production rate in source A alone is a factor of ~ 2 larger than that from the inner kiloparsec of M82 (Satyapal 1995).

In recent papers, the He I 2.06 μm/Brγ ratio has been used to estimate the effective temperature of the exciting stars and therefore the age of the stellar population or the upper mass cutoff of the IMF (see, e.g., Doyon, Puxley, & Joseph 1992). A low He I 2.06 μm/Brγ ratio can be indicative of a low upper mass cutoff or an older population of stars. However, radiative transfer effects result in a more complicated behavior of this ratio with effective temperature (Doherty et al. 1995; Shields 1993). These effects are significant at effective temperatures above $\sim$40,000 K, where the predicted He I 2.06 μm/Brγ ratio becomes a decreasing function of the temperature of the ionizing sources. Therefore, in some cases the effective temperature estimated from this ratio is ambiguous, requiring independent constraints to confirm. From Table 5, we see that the He I 2.06 μm/Brγ ratio is the lowest in source B. Since the CO index is high in this source and the Brγ equivalent width is low (see § 3.5), the low He I 2.06 μm/Brγ ratio can be attributed to a lower effective temperature for the stellar population in source B than in sources A and C. Although source C has a lower He I 2.06 μm/Brγ ratio than does source A, the absence of the 2.3 μm CO absorption feature, the high the Brγ equivalent width, and the possible detection of Wolf-Rayet features (Armus et al. 1989) from this source suggests that source C is characterized by a younger stellar population. The lower He I 2.06 μm/Brγ ratio therefore probably results from a higher effective temperature for the ionizing stars in source C compared with source A.

The radio properties of each of the sources in Arp 299 are also significantly different. The radio continuum emission in galaxies can generally be attributed to synchrotron (nonthermal) emission from supernova remnants or an active galactic nucleus and free-free (thermal) emission from

ionized gas. The radio emission from supernova remnants are observed to have power-law spectra with spectral indices in the range -0.1 to -1.0 (Green 1984). The nonthermal radio emission from active galactic nuclei on the other hand, often show flat or inverted spectra (see, e.g., Condon et al. 1982), which is generally attributed to synchrotron self-absorption in the dense, compact core. Optically thin free-free emission produces a $\alpha_{ff} = -0.1$ continuum spectrum at radio frequencies. We have used our recombination-line spectrophotometry to predict the thermal component of the 5 GH continuum. Assuming case B recombination and $T_e = 10^4$ K, the intrinsic Brγ line strength is related to the free-free continuum at 5 GHz by the relation:

$$F_{5\mathrm{GHz}}(\mathrm{Jy}) = 1.13 \times 10^{14} F_{\mathrm{Br}\gamma}(\mathrm{W\ m^{-2}})\ ;$$

(derived from Condon 1992). As can be seen from Table 5, the thermal contribution to the observed 5 GHz flux density is small in all sources, being the smallest in source A. The relatively flat radio spectrum in source A can therefore not be produced by free-free emission from ionized gas. It is compact, with a size of 60 pc as seen from recent VLA observations (Carral, Turner, & Ho 1990; Zhao et al. 1997), which suggests the possible presence of an active galactic nucleus. However, we see no evidence of broad near-infrared recombination line emission (see Fig. 4) and the recombination line ratios are consistent with case B recombination and extinction. In addition, source A has a large 3.29 μm feature flux, and the ratio of feature to far-infrared luminosity is consistent with that observed in most starburst galaxies, which suggests the dominance of starburst activity in this source. Sources B and C have resolved radio components and have spectral indices that can be easily explained by the combined effects of thermal emission from ionized gas and nonthermal emission from supernova remnants.

3.5. *A Starburst Model of Arp 299*

The results presented in this paper suggest a starburst origin for the observed activity in Arp 299. This galaxy appears to be undergoing an intense burst of star formation, similar to but more energetic than the one taking place in the prototypical starburst, M82. We have also shown that the observations suggest a difference in age or IMF at the positions of the three active sources in this galaxy. A more quantitative analysis of these hypotheses can be carried out using the stellar population models discussed in Satyapal et al. (1997). These models assume an instantaneous starburst with a stellar population characterized by a Salpeter IMF (Salpeter 1955) between 1 and 100 $M_\odot$.

The starburst age corresponding to the three sources can be inferred from the observed CO indices and Brγ equivalent widths as has been done previously for a number of galaxies (see, e.g., Doyon, Joseph, & Wright 1994; Satyapal et al. 1997). These observations are particularly well suited to constraining the age of a stellar population since the model quantities show a sharp change in a short time interval and are relatively insensitive to the assumed IMF of the population. We used the Brγ equivalent width, W(Brγ), from the stellar population models discussed in Leitherer & Heckman (1995). As can be seen from Figure 6, the CO index is anticorrelated with W(Brγ) and comparison of these observed values with our starburst model (Fig. 7) identifies these regions as starbursts and provides information on their age.

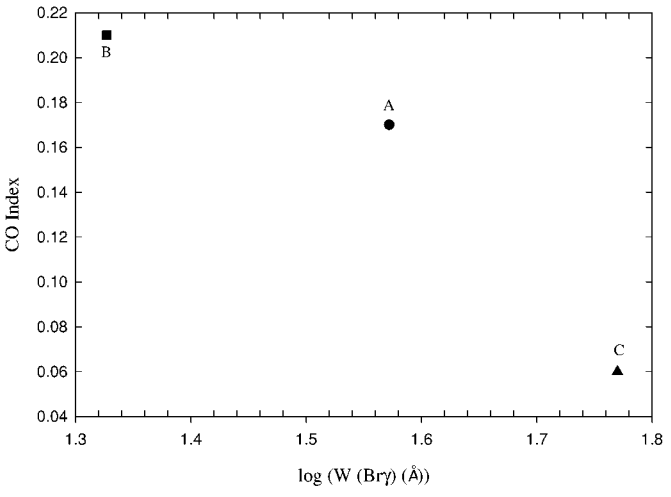

FIG. 6.—Observed CO index vs. W(Brγ) in Arp 299

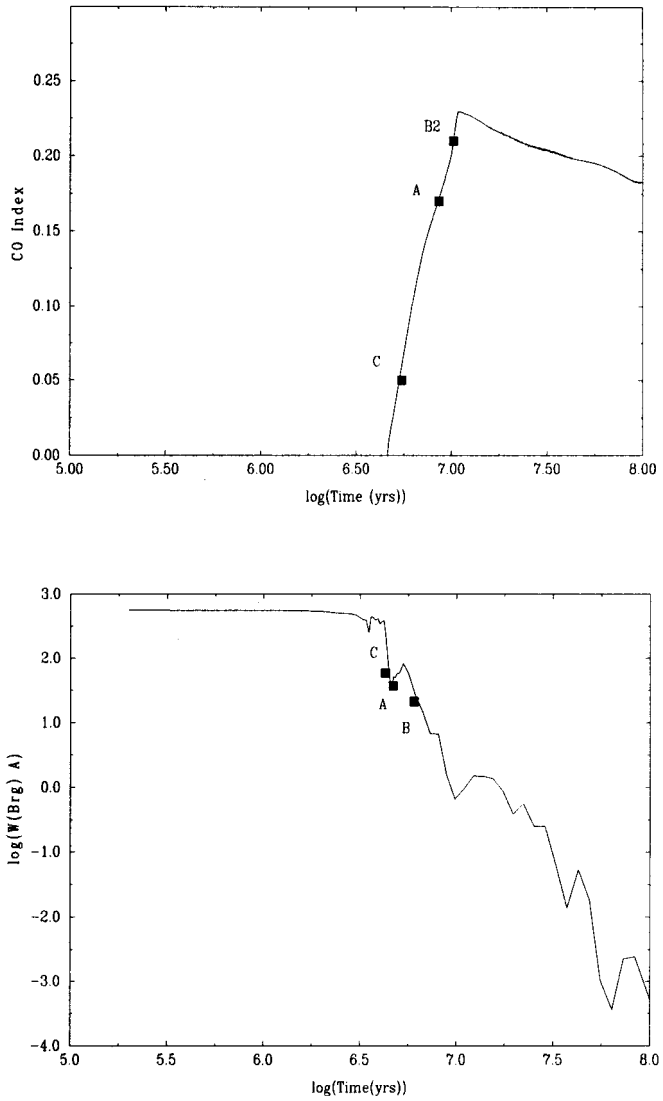

FIG. 7.—CO index and W(Brγ) as a function of time for a starburst model with $m_L = 1\ M_\odot$ and $m_U = 100\ M_\odot$ together with the intersections of the observed values of sources A, B, and C in Arp 299.

The observed CO indices imply ages of $\sim 6 \times 10^6$, 8×10^6, and 4×10^6 for sources A, B, and C, respectively, very similar to those inferred from the observed Brγ equivalent widths (5×10^6,7×10^6, and 4×10^6). These ages are typical of the inferred ages for the 12 pointlike sources in M82 (Satyapal et al. 1997) and for starburst galaxies in general. The observed CO indices and Brγ equivalent widths imply that source B is older than source A and source C is the youngest star forming region. In the previous section we have outlined the various observations that suggest that source C is the youngest starburst. Source A, however, has the largest ratio of far-infrared luminosity to ionizing flux (see Table 5), which has led several authors to suggest that the starburst taking place in this source is the oldest (see, e.g., Telesco et al. 1985) or that a large fraction of the far-infrared luminosity in this source is powered by an active galactic nucleus (see Lonsdale & Smith 1995). However, we have detected emission from the 3.29 μm dust feature from this source, and the ratio of feature to far-infrared luminosity is consistent with that observed in most starburst galaxies. Furthermore, we have found no evidence for broad hydrogen recombination lines from this source. Using the starburst parameters derived for source A, the implied supernova rate in this source is ~ 0.6 yr^{-1}. We can estimate the resulting nonthermal radio flux density from source A and compare it to the observed value listed in Table 5. Using the expression deduced from Huang et al. (1994) from observations of M82.

$$\nu_{\rm SNR}({\rm yr}^{-1}) = 3.4 \times 10^{-6} F_{5\,{\rm GHz}}({\rm mJy}) D^2_{\rm Mpc} ,$$

where $F_{5\,{\rm GHz}}$(mJy) is the nonthermal radio flux density at 5 GHz for a galaxy at distance D in megaparsecs, we find that the derived radio flux density from supernova remnants in source A is ~ 100 mJy, comparable to the nonthermal component of the observed 5 GHz flux density. Thus, our data suggest that the existence of an AGN is not necessary to explain both the radio properties of source A and the bulk of the far-infrared luminosity. Our observations suggest instead that the upper mass cutoff in source A is smaller than it is in source B. Fewer massive stars would reduce the ionizing flux without necessarily decreasing the total far-infrared luminosity.

Thus our simple starburst model suggests that sources A, B, and C are all undergoing intense starburst episodes. The starburst in source B is older than that in source A and source C is the youngest starburst region. Source A appears to have a smaller upper mass-cutoff than source B, which explains the larger ratio of far-infrared luminosity to ionizing flux observed from this source.

4. SUMMARY

In this paper, we have presented the results of our near-infrared Brγ and Paβ Fabry-Perot, near-infrared broadband, and 3.29 μm dust feature imaging observations of the Arp 299 system. These data have been used to show the following:

1. The near-infrared hydrogen recombination line, the 3.29 μm dust feature, and the near-infrared broadband emission is concentrated at the positions of three active regions, known as sources A, B, and C. This morphology is consistent with that at 10 μm and 6 cm and can be understood as the combined effects of young massive stars, a population of supergiants, and supernova remnants.

2. Assuming a foreground screen geometry, the extinction, A_V, toward the ionized gas in sources A, B, and C is ~ 6, 6, and 2 mag, respectively. This was derived using the Brγ/Paβ flux ratio and the assumption of case B recombination.

3. Emission from the 3.29 μm dust feature has been detected from each of the three sources. The ratio of the total far-infrared luminosity to the extinction-corrected feature luminosity is found to be consistent with that found in M82 and many other starburst galaxies. In source A, $L_{\rm FIR}/L_{3.3}$ is 3280 using the observed feature flux and 1840 using the extinction-corrected flux. In sources B and C combined, $L_{\rm FIR}/L_{3.3}$ is 1650 using the observed feature flux and 1550 after correcting for extinction. The extinction-corrected value in M82 is 1340. The 3.29 μm dust feature is a better indicator of the far-infrared luminosity in Arp 299 than Brγ. The extinction-corrected far-infrared to Brγ luminosity ratio is 7.0×10^4 in source A and 2.6×10^4 in sources B and C combined, compared to the value of 1.4×10^4 in M82.

4. Our recombination-line images were used to estimate separately the contribution to the near-infrared continuum bandpasses from nebular emission. These sources of emission are found to be most significant in source C but do not contribute appreciably to the total near-infrared continuum in any of the sources.

5. The near-infrared colors of sources A and B are very similar to those found in the M82 starburst complex, and starburst galaxies in general. These colors can be ascribed to a normal population of stars and some assumed dust geometry. Source C, however, has a very unusual color that cannot be ascribed to extinction from any assumed dust geometry. The unusual color of this source may be the result of a population of Wolf-Rayet stars. The dust geometry in Arp 299 is probably more complicated than it is in, e.g., M82; a foreground screen geometry will most likely result in less reliable estimates for the extinction toward the broadband emission.

6. When compared with our starburst models, the observed CO indices and Brγ equivalent widths of these sources imply ages similar to those inferred for the M82 starburst complex and starburst galaxies in general.

7. Comparison of our simple starburst model with observations suggests that sources A, B, and C are all undergoing intense starburst episodes. The starburst in source B is older than that in source A and source C is the youngest starburst region. Source A appears to have a smaller upper mass-cutoff than source B, which explains the larger ratio of far-infrared luminosity to ionizing flux observed from this source.

8. Our observations can be explained entirely by a starburst model for the Arp 299 system. The putative AGN in source A does not dominate the properties of this source. We see no evidence of broad recombination lines. In addition, the ratio of feature to far-infrared luminosity is consistent with that observed in most starburst galaxies, which suggests that the large far-infrared luminosity from this source can be completely attributable to starburst activity.

The authors would like to acknowledge the support of the Smithsonian Garber Fellowship program, the National Research Council, the Office of Naval Research, NASA, and NSF. We are also very grateful for the insightful discussions with Larry Helfer and Mark Wardle, and the helpful comments from the anonymous referee.

REFERENCES

Armus, L., Heckman, T. M., & Miley, G. K. 1989, ApJ, 347, 727
Beck, S. C., Turner, J. L., & Ho, P. T. P. 1986, ApJ, 309, 70
Bushouse, H. A., & Gallagher, J. S. I. 1984, PASP, 96, 273
Carral, P., Turner, J. L., & Ho, P. T. P. 1990, ApJ, 362, 434
Cole, L. J. 1996, M.S. thesis, Univ. Wyoming
Condon, J. J., Condon, M. A., Gisler, G., & Puschell, J. J. 1982, ApJ, 252, 102
Condon, J. J. 1992, ARA&A, 575
Dennefeld, M., & Desert, F. X. 1990, A&A, 227, 379
de Vaucouleurs, A., & de Vaucouleurs, G. 1967, AJ, 72, 730
Doherty, R. M., Puxley, P. J., Lumsden, S. L., & Doyon, R. 1995, MNRAS, 277, 577
Doyon, R., Joseph, R. D., & Wright, G. S. 1994, ApJ, 421, 101
Doyon, R., Puxley, P. J., & Joseph, R. D. 1992, ApJ, 397, 117
Draine, B. T. 1989, in Infrared Spectroscopy in Astronomy, ed. B. H. Kaldeich (Noordwijk: ESTEC), 93
Elias, J. H., Frogel, J. A., Matthews, K., & Neugebauer, G. 1982, AJ, 87, 1029
Fischer, J., Smith, H. A., & Glaccum, W. 1990, in ASP Conf. Ser. 14, Astrophysics with Infrared Arrays, ed. R. Elston (San Francisco: ASP), 63
Frogel, J. A., Persson, S. E., Aarson, M., & Matthews, K. 1978, ApJ, 220, 75
Gehrz, R. D., Sramek, R. A., & Weedman, D. W. 1983, ApJ, 267, 551 GSW
Green, D. A. 1984, MNRAS, 209, 449
Greenhouse, M. A., et al. 1997, ApJ, 476, 105
Huang, Z. P., Thuan, T. X., Chevalier, R. A., Condon, J. J., & Yin, Q. F. 1994, ApJ, 424, 114
Hummer, D. G., & Storey, P. J. 1987, MNRAS, 224, 801
Joy, M., Lester, D. F., Harvey, P. M., Telesco, C. M., Decher, R., Rickard, L. J., & Bushouse, H. 1989, ApJ, 339, 100
Keto, E., et al. 1997, ApJ, 485, 598
Kleinmann, S. G., & Hall, D. N. B. 1986, ApJS, 62, 501
Koornneef, J. 1983, A&A, 128, 84
Landini, M., Natta, A., Oliva, E., Salinari, P., & Moorwood, A. F. M. 1984, A&A, 134, 384
Leitherer, C., & Heckman, T. M. 1995, ApJS, 96, 9
Lonsdale, C. J., & Smith, H. E. 1995, ApJ, 438, 632
Mazzarella, J. M., Voigt, G. M., Soifer, B. T., Matthews, K., Graham, J. R., Armus, L., & Shupe, D. 1994, AJ, 107, 1274
Miles, J. W., Houck, J. R., & Hayward, T. L. 1994, ApJ, 425, L37
Mizutani, K., Suto, H., & Maihara, T. 1989, ApJ, 346, 675
———. 1994, ApJ, 421, 475
Mouri, H., Kawara, K., Taniguchi, Y., & Nishida, M. 1990, ApJ, 356, L39
Nelson, K., et al. 1999, in preparation
Nakagawa, T., Nagata, T., Geballe, T. R., Okuda, H., Shibai, H., & Matsuhara, H. 1989, ApJ, 340, 729
Ridgway, S. E., Wynn-Williams, C. G., & Becklin, E. E. 1994, ApJ, 428, 609
Salpeter, E. E. 1955, ApJ, 121, 161
Sanders, D. B., & Mirabel, I. F. 1985, ApJ, 298, L31
———. 1996, ARA&A, 34, 749
Sargent, A. I., Sanders, D. B., Scoville, N. V., & Soifer, B. T. 1987, ApJ, 312, L35
Satyapal, S. 1995, Ph.D. thesis, Univ. Rochester, Rochester
Satyapal, S., et al. 1995, ApJ, 483, 148
Satyapal, S., Watson, D. M., Pipher, J. L., Forrest, W. J., Greenhouse, M. A., Smith, H. A., Fischer, J., & Woodward, C. E. 1997, ApJ, 448, 611
Sellgren, K., Werner, M. W., & Dinerstein, H. L. 1983, ApJ, 271, L13
Shields, J. C. 1993, ApJ, 419, 181
Shier, L. M., Rieke, M. J., & Rieke, G. H. 1994, ApJ, 433, L9
Soifer, B. T., Sanders, D. B., Madore, B. F., Neugebauer, G., Danielson, G. E., Elias, J. H., Lonsdale, C., & Rice, W. L. 1987, ApJ, 320, 238
Stark, A. A. 1997, ApJ, 481, 587
Telesco, C. M., Decher, R., & Gatley, I. 1985, ApJ, 299, 896
Tokunaga, A. T., Sellgren, K., Smith, R. G., Nagata, T., Sakata, A., & Nakada, Y. 1991, ApJ, 380, 452
Toomre, A., & Toomre, J. 1972, ApJ, 178, 623
Williams, P. M., Van der Hucht, K. A., & The, P. S. 1987, A&A, 182, 9L
Wynn-Williams, C. G., Hodapp, K.-W., Joseph, R. D., Eales, S. A., Becklin, E. E., McLean, I. S., Simons, D. A., & Wright, G. S. 1991, ApJ, 377, 426
Zhao, J.-H., Anantharamaiah, K. R., Goss, W. M., & Viallefond, F. 1997, ApJ, 482, 186